

Homophily Within and Across Groups

Abbas K. Rizi,^{1,2,3} Riccardo Michielan,^{4,5} Clara Stegehuis,⁴ and Mikko Kivelä³

¹*DTU Compute, Technical University of Denmark, Lyngby, Denmark*

²*Center for Social Data Science, University of Copenhagen, Denmark*

³*Department of Computer Science, School of Science, Aalto University, Espoo, Finland*

⁴*Faculty of Electrical Engineering, Mathematics and Computer Science, University of Twente, Enschede, Netherlands*

⁵*Gran Sasso Science Institute, L'Aquila, Italy*

(Dated: June 11, 2025)

Homophily—the tendency to connect with similar others—plays a central role in shaping network structure and function. It is often treated as a uniform, global parameter, independent from other structural features. Here, we propose a maximum-entropy framework that decomposes homophily into contributions within and across groups, with the stochastic block model emerging as a special case. Our exponential-family formulation, parameterized by group size, fits real-world social networks well and allows homophily to be captured with a single parameter per group size. This decomposition shows that aggregate metrics often obscure group-level variation. We also find that the scale-dependent distribution of homophily has a significant impact on network percolation, influencing epidemic thresholds, the spread of ideas or behaviors, and the effectiveness of intervention strategies. Ignoring this heterogeneity can lead to distorted conclusions about connectivity and dynamics in complex systems.

I. INTRODUCTION

Homophily—the tendency to interact with similar others—shapes both the structure and function of networks [1–5]. In social systems, people tend to connect with others who share attributes such as sex, age, race, occupation, sexual preferences, socioeconomic background, or vaccination status [6–16]. Assortative mixing occurs in various settings, ranging from friendships and workplace ties to online platforms, peer influence networks [17–20], and even graph neural networks [21–24]. It shapes interactions and governs processes like contagion, diffusion, and coordination [25–29]. In healthcare settings, the close contact between healthcare workers and vulnerable patients can alter outbreak patterns, as homophily interacts with variations in infectiousness and susceptibility, reshaping epidemic dynamics [30–37].

Homophily varies by interaction type and tie strength [38–40]. Strong ties tend to form within close-knit groups, while weak ties more often bridge distant or dissimilar clusters [39, 41]. Networks of citations and trade partnerships typically exhibit dual mixing patterns, combining dense local collaboration with broad cross-group exchange [42, 43]. Gender homophily, in particular, is sensitive to both medium and group size. On Instagram, women show strong same-gender preferences in comments, while men are largely neutral [44]. In face-to-face proximity networks, women tend to form homophilic triads, whereas men favor same-sex dyads [45]. In contrast, the teen-focused Spanish social network Tuenti shows the opposite: women sustain stronger same-gender dyads, and men more often form all-male triads than expected under null models [46].

These observations indicate that homophily is influenced by both group composition and size [47], highlighting its variability across social scales [48]. Small, cohesive groups often display high local homophily, whereas long-

range connections mix more randomly, producing distinct within- and across-group connectivity essential for understanding collective behavior [49]. Nevertheless, many network models simplify homophily into a single, uniform parameter—essentially a summary statistic that captures only the network’s average mixing pattern [14, 25, 50–54]. Epidemiological studies emphasize the importance of this complexity, demonstrating that high within-group homophily can elevate epidemic thresholds, while increased cross-group interactions typically lower them [6, 55–59]. Thus, to improve our understanding of network formation and dynamics, we must model homophily as a heterogeneous quantity across social scales.

We introduce a network model in which groups, modeled as cliques, exhibit homophily that varies with group size. Using a maximum-entropy framework, the model captures homophilic structure beyond pairwise links and distinguishes between within- and across-group connections. This reveals scale-dependent patterns often overlooked by standard measures and aligns well with empirical studies. Our results show that such multi-scale homophily can raise or lower the percolation threshold, depending on how intra- and inter-group links are distributed. These findings offer new tools for understanding epidemic thresholds, designing interventions, and modeling the spread of information or behavior in social systems.

The remainder of the paper is structured as follows. Section II describes our network model and demonstrates how it encodes multi-scale homophily. Section III validates the model using real-world data, illustrating how within- and across-group mixing patterns emerge under the same modeling assumptions. Section IV examines how multi-scale homophily influences percolation thresholds and network connectivity, with implications for epidemic control and other contagion processes.

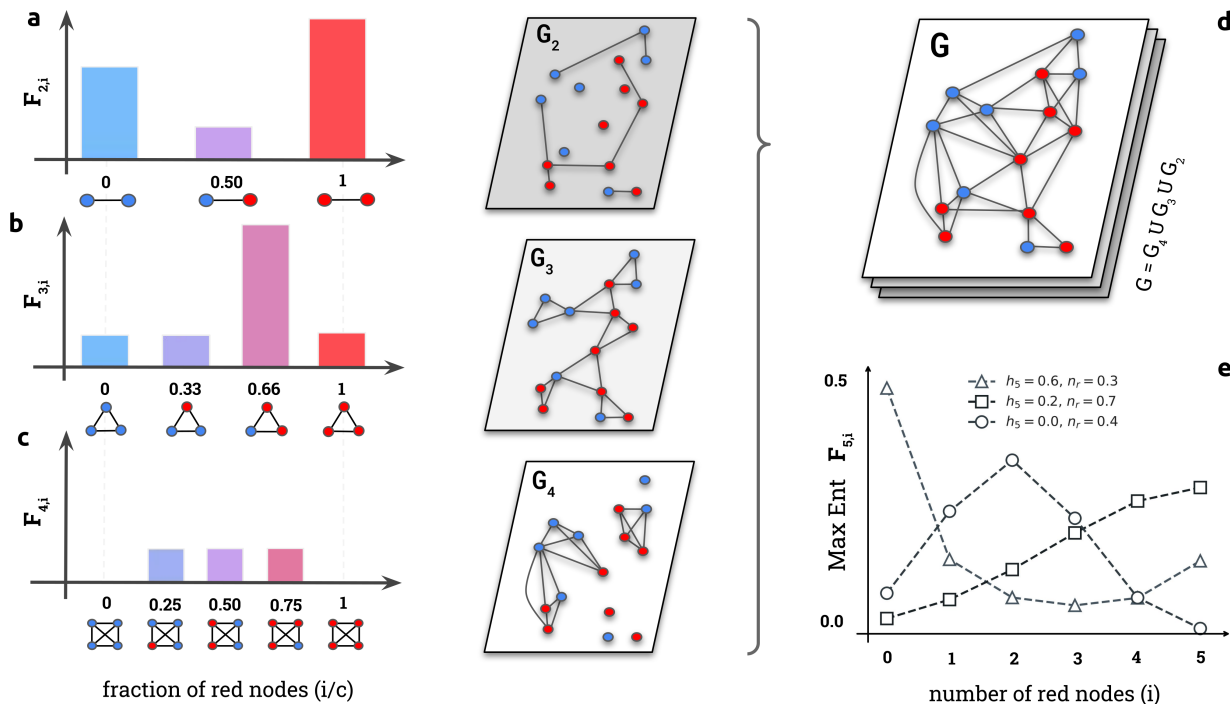


FIG. 1. **Constructing a Homophilic Clique Network with Eight Red and Seven Blue Nodes.** With two colors, each c -clique can appear in $c + 1$ different compositions, distributed according to F_c . (a-c) The network G is constructed by merging multiple clique layers—specifically, 2-, 3-, and 4-cliques—where each layer G_c contains cliques of size c but shares the same set of nodes. While the nodes remain fixed, each layer differs in clique size c and composition distribution F_c . The accompanying histograms show the frequency of each c -clique type in the network G_c . In each layer, M_c groups of c nodes are sampled with replacement from the available colored nodes and converted into c -cliques. For example, G_3 consists of seven sampled 3-cliques, while G_2 is constructed similarly, but with its own parameters M_2 and F_2 . (d) All layers are then merged to form the final network: $G = \bigcup G_c$. (e) The maximum-entropy clique composition distribution F_5 , derived from Eq. (8), is illustrated for cliques of size $c = 5$ at homophily levels $h_5 = 0.2$ and $h_5 = 0.6$, across several values of the red-node fraction n_r . For clarity, we omit the corresponding networks generated from these distributions. More details in Sec. II.

II. MODEL DESCRIPTION

We introduce a network model that captures homophily at different social scales. The model generates an undirected, sparse graph G , formed as the union of multiple subnetworks $\{G_c\}$, all sharing the same set of nodes. Each subnetwork G_c consists of cliques of size c (groups). Every node in the network has a discrete attribute—for example, a categorical label indicating membership. We begin with a binary labeling of nodes as red or blue, extending to multiple classes in Sec. VD. As shown in Fig. 1, the network consists of N nodes, with N_r red and $N_b = N - N_r$ blue. Their corresponding proportions are $n_r = N_r/N$ and $n_b = 1 - n_r$. All subnetworks G_c share the same node set; that is, red and blue labels are consistent across layers.

We classify the cliques within each subnetwork G_c based on the number of red or blue nodes they contain. A c -clique can be classified into one of $c + 1$ types, that are specified by the number i of red nodes included. We denote by $F_{c,i}$ the proportion of c -cliques in G_c that contain exactly i red nodes and $c - i$ blue nodes. To ensure that the overall fraction of red and blue nodes

is preserved in the large-network limit, the distributions $\{F_{c,i}\}$ must satisfy

$$\sum_{i=0}^c \frac{i}{c} F_{c,i} = n_r, \quad \sum_{i=0}^c \frac{c-i}{c} F_{c,i} = n_b. \quad (1)$$

To construct each subnetwork G_c , we independently sample M_c cliques of size c from the total population of nodes according to the distribution $\{F_{c,i}\}$. Fig. 1(a-c) illustrates the construction of three subnetworks with different clique-type distributions. In this framework, G_1 is a trivial graph of isolated colored nodes, and G_2 is a two-block stochastic block model [60]. The final network G , as shown in Fig. 1d, is obtained by merging all subnetworks;

$$G = \bigcup_c G_c. \quad (2)$$

Since cliques are sampled independently, setting $M_c = \mathcal{O}(N)$ ensures that each layer G_c remains sparse and that the fraction of overlapping links vanishes in the large-network limit. Given a prescribed average degree $\langle d \rangle$, controlling M_c allows us to regulate the number of links from each clique size to the overall network. In practice, we sample fewer large cliques, reflecting empirical

observations: larger cliques tend to be rarer in real-world networks due to cognitive and social constraints—a phenomenon known as “schisming” [61, 62]. A more detailed discussion regarding finiteness and empirical networks is provided in Sec. VB.

A. Group Homophily Values

A standard global measure for quantifying how nodes with categorical attributes (such as color) tend to connect is the *Coleman index*, also known as the *assortativity coefficient* [63–65]. It is defined as

$$h = \frac{\sum_k (e_{kk} - n_k^2)}{1 - \sum_k n_k^2} = \frac{e_{rr} + e_{bb} - n_r^2 - n_b^2}{1 - n_r^2 - n_b^2}, \quad (3)$$

where e_{rr} and e_{bb} are the fractions of red–red and blue–blue links, and n_k is the fraction of nodes of color k . The numerator in Eq. 3 corresponds to modularity, while h is modularity normalized by its maximum value [66, 67]. By construction, $|h| \leq 1$: values near 1 signal strong homophily or segregation; $h \approx 0$ indicates random mixing; and negative values imply heterophily [68].

In our framework, cliques are sampled independently, and each node participates in a Poisson-distributed number of cliques. Under these assumptions, the Coleman index (3) can be decomposed into contributions from each clique layer G_c , giving

$$h = \sum_{c \geq 2} \alpha_c h_c, \quad (4)$$

where h_c denotes the homophily of G_c , and α_c is the fraction of links contributed by layer G_c . Consider a network G constructed from two layers, G_2 and G_6 . Here, h_2 quantifies across-group homophily and h_6 captures within-group homophily, assuming the groups are defined by the 6-cliques. The total homophily becomes $h = \alpha_2 h_2 + \alpha_6 h_6$, with each layer’s influence determined by its corresponding α_c . For instance, $\alpha_2 = \alpha_6 = 0.5$ gives equal weight to both layers, whereas $\alpha_2 > \alpha_6$ results in across-group homophily dominating, and vice versa. In general, the weights α_c can be computed as

$$\alpha_c = \frac{c(c-1)}{N\langle d \rangle} M_c. \quad (5)$$

Each h_c can further be decomposed into the weighted average of homophily contributions $h_{c,i}$ from all c -cliques with i red nodes:

$$h_c = \sum_{i=0}^c h_{c,i} F_{c,i}. \quad (6)$$

$h_{c,i}$ measures the deviation of such a c -clique’s composition from random mixing and is defined as

$$h_{c,i} = \frac{\binom{i}{2} + \binom{c-i}{2} - n_r^2 - n_b^2}{1 - n_r^2 - n_b^2}. \quad (7)$$

This equation defines homophily at the clique level, following the Coleman approach. It is worth noting that Eq. 3 can also be decomposed into contributions at the node or neighborhood level, where “node congruity” measures each node’s share of the overall homophily [48, 69, 70]. However, the formalism presented above provides sufficient measures for this study.

B. Maximum Entropy Distribution

Since many different $F_{c,i}$ distributions can produce the same overall homophily h_c , we use a *maximum entropy* approach to identify the least-biased distribution consistent with the desired group homophily h_c and the red and blue node fractions n_r and n_b . Specifically, we choose $F_{c,i}$ to maximize entropy subject to two constraints: (i) the average fraction of red nodes in cliques equals n_r (Eq. (1)); and (ii) the resulting clique-layer homophily is h_c (Eq. (6)). Since the network contains only two colors, satisfying constraint (i) automatically ensures that the blue-node fraction $n_b = 1 - n_r$ is preserved, so only one constraint is needed to fix both. The resulting distribution takes the exponential-family form:

$$F_{c,i} = \frac{1}{Z} \exp(\theta_r i + \theta_{h_c} h_{c,i}), \quad (8)$$

where Z is the partition function normalizing over all c -clique compositions. The parameters θ_r and θ_{h_c} emerge naturally as Lagrange multipliers in our maximum-entropy formulation [71]: θ_r sets the fraction of red nodes, while θ_{h_c} tunes the homophily level h_c . These parameters are commonly referred to as *conjugate couplings* in statistical mechanics. This approach naturally accommodates networks with different degrees of mixing and handles both symmetric and skewed attribute distributions. Fig. 1e shows three examples from this versatile family of distributions.

Analogous to spin models on hyperedges [72–74], our framework can be viewed as a canonical ensemble, where clique homophily and color composition act as soft constraints—similar to inverse-temperature-like parameters in a spin system defined on a hypergraph. Each clique configuration corresponds to a microstate, weighted by a Boltzmann factor $F \sim e^{-\mathcal{H}}$. In this formulation, the Hamiltonian \mathcal{H} depends on the full color composition of each clique. A c -clique thus represents a higher-order interaction among the spins (i.e., node attributes) of its c members.

This two-color framework easily generalizes to multiple categorical attributes and even multidimensional homophily, allowing more attributes to be considered simultaneously. Sections VD and VE detail these generalizations explicitly.

III. RESULTS

To assess how well our model captures homophilic structure in real-world networks, we analyze six datasets with categorical node attributes: the Slovak social networking site Pokec [75], the Copenhagen Networks Study (CPH) [76], the music-sharing platform Last.fm [77], a mobile phone call network [78, 79], the face-to-face proximity dataset SocioPatterns [45, 80], and 100 Facebook friendship networks [81]. These datasets, summarized in Table I, span a broad spectrum of social interaction types—from digital connections to physical encounters.

For each empirical network G , we extract all maximal cliques and group them by size to form distinct layers $\{G_c\}$. As shown in Fig. 1(a–d), this decomposition yields a family of subgraphs, each capturing interactions at a specific clique size. Some links appear in multiple layers, but this redundancy has a negligible effect on measured homophily. We fit the maximum-entropy model (8) to the observed clique-type distributions by maximizing the likelihood, thereby estimating the parameters $\{\theta\}$. For details on edge duplication and its impact, see Sec. V B.

Our maximum-entropy approach closely matches the empirical distributions of clique compositions, as illustrated in Fig. 2a. Similar to Fig. 1, it compares observed histograms of F_c across several empirical networks with the model fits from Eq. (8). With only two parameters—the expected homophily h_c and the fraction of nodes of one type—the model accurately captures the full distribution of clique compositions F_c in our empirical data. This means that h_c values contain all the information about the complete distributions F_c of our data, and it is enough to report the h_c values to fully describe how the homophily is distributed within and across groups of different sizes.

Although these networks differ in global properties, such as degree distributions that do not necessarily align with those generated by our model, the method still effectively reproduces the patterns of homophily. This robustness stems from the fact that the model is directly constrained by empirical clique compositions or homophily values, rather than by assumptions about the degree sequence or other global network characteristics.

Total Coleman indices range from mildly homophilic ($h = 0.1$ in the Last.fm network and $h = 0.2$ in the University of Oklahoma Facebook network), to randomly mixed ($h = 0.0$ in the CPH and SocioPatterns networks), and mildly heterophilic ($h = -0.2$ on the Pokec platform). However, these aggregate measures conceal substantial variation at the clique level. We observe diverging trends across datasets. In the mildly homophilic networks, homophily increases with clique size: Last.fm exhibits random mixing for dyads ($h = 0$) but stronger homophily in larger cliques ($h = 0.3$); Oklahoma shows heterophily among bridging links ($h = -0.2$) and homophily only in larger groups. In contrast, CPH and SocioPatterns—despite appearing randomly mixed overall—display the opposite pattern: bridging links are ho-

Dataset	Link Type	n_r (%)	h	N
Mobile Phone	Phone Calls	55.1	0.1	2,173,030
Pokec	Friendship	46.6	-0.2	383,943
Last.fm	Friendship	68.3	0.1	188,672
Oklahoma FB	Friendship	49.3	0.2	16,245
CPH	Proximity, Calls, etc.	78.1	0.0	779
SocioPatterns	Proximity	57.4	0.0	115

TABLE I. Summary of datasets used in this study. The variable n_r represents the relative size of the red (male) group. The Coleman index h is for overall sex homophily.

mophilic, but larger cliques are heterophilic.

The Pokec network offers a particularly striking example of a pattern behind an average index. Its Coleman index $h = -0.2$ suggests mild heterophily, yet dyads (G_2) exhibit strong cross-sex preference with $h_2 = -0.6$. As clique size increases from 2 to 10, this intermingling turns into homophily. This transformation is not a minor refinement—it fundamentally changes the interpretation of the network: pairwise links reflect Pokec’s dating-oriented function, while larger cliques reflect its broader role as a social media platform where, at social scales, *birds of a feather flock together* [1].

Facebook data from 100 U.S. universities and colleges offers a socially comparable set of environments with rich attribute annotations. Altenburger et al. [82] previously showed that users tend to form highly sex-homogeneous friendship circles—often all-male or all-female—even though these preferences largely cancel out in aggregate, producing weak overall homophily. Fig. 2(c–e) illustrates how homophily varies with clique size when nodes are grouped by (c) sex, (d) student status, and (e) class year. Each attribute captures different social dynamics, leading to distinct homophily profiles. In Fig. 2c, sex-based homophily increases monotonically with clique size, suggesting that sex-based clustering intensifies in larger groups. In contrast, Fig. 2d shows an average trend with a medium level of homophily at the link level and only a slight dependency on group size.

Our framework can analyze more complex scenarios involving multiple non-binary attributes. Fig. 2e reveals a clearly non-monotonic pattern for class year in the Facebook network: homophily rises in smaller cliques but levels off as groups grow, likely reflecting increased mixing between cohorts in broader social circles. Notably, similar multiscale mixing patterns have been reported by Peel et al. [48], who demonstrated that even when the network exhibits modest overall homophily, certain subgroups (such as first-year students) display markedly higher local homophily.

These observations shed a new light on findings by Traud et al. [81], who showed that communities in university Facebook networks tend to cluster by class year. Our analysis reveals that smaller cliques strongly reflect

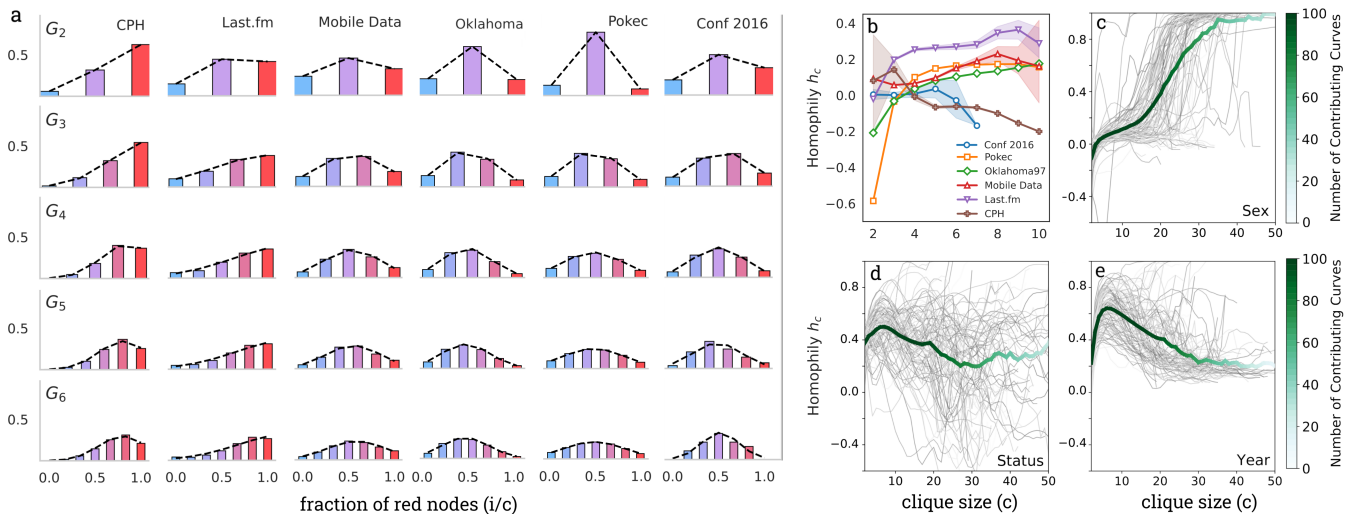


FIG. 2. **Empirical and Theoretical Distributions of Clique Types and Homophily in Real-world Networks mentioned in Sec. III.** (a) Each column compares empirical clique-type distributions (histograms) with the corresponding maximum-entropy distributions (dashed lines, computed using Eq. (8)), showing strong agreement and validating the model’s accuracy in capturing observed clique compositions across real-world datasets. Red represents males and blue, females. (b) Variation in homophily values h_c across clique sizes (up to $c = 10$) for several empirical networks, highlighting distinct group interaction patterns based on sex attributes. Error bars represent 95% confidence intervals obtained via bootstrap resampling. (c–e) Average homophily trends across clique sizes for Facebook friendship networks from 100 U.S. institutions, with attributes grouped by: (c) Sex (two categories), (d) Student status (two categories), and (e) Class year (12 categories). Gray background curves represent individual institutions, while colored lines indicate the average trends. Lighter colors reflect a greater number of contributing institutions, emphasizing both inter-institutional variability and how homophily depends on the attribute under consideration.

graduation-year homophily, but this pattern weakens in larger groups, where other attributes—such as sex or student status—become more prominent. Similar scale-dependent patterns are well documented in the broader sociological literature. Homophily is shaped by multiple, context-dependent mechanisms [1]; academic performance influences how students reorganize their friendships [83]; and ethnic background plays a significant role in network formation in educational settings [84].

IV. PERCOLATION

The structure of the network determines how robust it is to being disintegrated into small, connected components when links or nodes are removed [85–89]. In social systems, these removals can stem from communication failures, a limited number of contacts, or other reasons, and the connectivity then determines the spread of ideas, behaviors, or diseases [38, 90].

Removing across-group links—often corresponding to weak ties that bridge otherwise separate communities [91]—can trigger sudden fragmentation, severing pathways across the network. In contrast, losing within-group links, typically associated with strong local ties within groups, tends to undermine cohesion within groups without immediately disrupting global connectivity [92–94]. This distinction is central to our analysis, where we explicitly differentiate between links that connect groups

(the G_2 -layer of our model) and those that bind them internally (the G_c layers for $c > 2$).

To show how group homophily values $\{h_c\}$ influence network behavior, we analyze their effect on connectivity and percolation thresholds. Since our model generates networks with nearly identical degree distributions across different homophily settings, any changes in percolation, such as shifts in the largest connected component or the threshold, reflect structural correlations induced by homophily, not degree variation [95]. This setup isolates the specific role of homophily within and across groups in shaping network robustness and percolation dynamics.

A. Colored Percolation

In a standard bond percolation process [85], each link in a network G is retained with probability ϕ and removed with probability $1 - \phi$, independently and *uniformly* at random. As ϕ varies, we track the size of the giant component—the largest connected subgraph—to study how connectivity responds to random removal of links. This process is relevant to various simple dynamics such as epidemics, information spreading, or behavior adoption, where deleted links represent blocked transmission paths. For example, in the case of epidemic spreading, under certain assumptions, the giant component corresponds precisely to the final outbreak size [94, 96]. As the disease becomes more infectious, ϕ increases, and the population

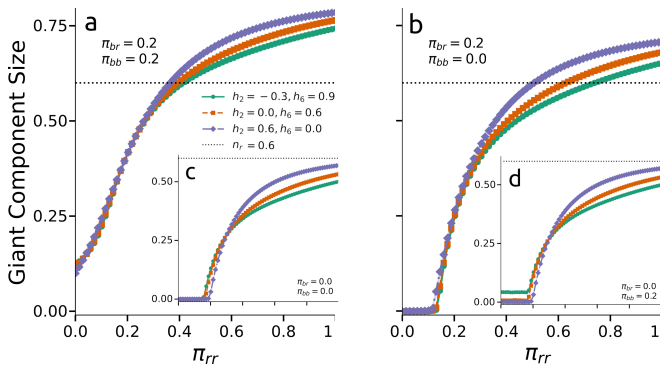


FIG. 3. Percolation Phase Transition in Networks with Different within- and across-homophily Values. Local mixing patterns affect the size of the giant component and the percolation threshold. Panels (a–d) show the percolation transition in the size of the giant component for networks composed of 2- and 6-cliques ($G = G_2 \cup G_6$). Each curve corresponds to a different pair of homophily levels, h_2 and h_6 , and tracks the growth of the giant component as the red–red link activation probability π_{rr} increases. Link activation settings vary across panels: (a) $\pi_{rb} = \pi_{bb} = 0.2$; (b) $\pi_{rb} = 0$, $\pi_{bb} = 0.2$; (c) $\pi_{rb} = 0$, $\pi_{bb} = 0$; and (d) $\pi_{rb} = 0.2$, $\pi_{bb} = 0$. All networks are generated with $N = 500,000$ nodes, average degree six, red node fraction $n_r = 0.6$, link composition $\alpha = 0.5$, and Coleman index $h = 0.3$. Results are averaged over 20 realizations. In (a), all networks remain in the supercritical regime regardless of π_{rr} , indicating that an average degree of six is sufficient for global connectivity under moderate homophily. By contrast, in (b) and (d), the percolation order of the curves reverses: the configuration that percolates last in (b) is the first to do so in (d). This reversal highlights how activating within- versus across-group links reshapes the percolation threshold, even when the overall homophily index remains fixed.

undergoes a continuous phase transition from a contagion-free to an endemic state. In more complex scenarios, link removal is not uniform and depends on node attributes. For example, disease transmission probabilities can differ based on age or vaccination status in a partially vaccinated population [14, 97–104]. In such cases, percolation is no longer governed by a single parameter ϕ , but by a vector of link-type-specific probabilities. In our colored network model, we remove links based on a vector $(\pi_{rr}, \pi_{rb}, \pi_{bb})$, where π_{kj} is the probability of removing a link between nodes of colors k and j [105]. In the large-network limit, this is equivalent to independently removing each kj -type link with probability π_{kj} . This is similar to the idea of neighbor-induced immunity percolation [106]. By varying these probabilities and observing how the giant component changes, we identify when the network undergoes a phase transition in connectivity.

Now, consider a network where red–blue and blue–blue links remain active with fixed probabilities, while the activation probability of red–red links varies from 0 to 1. In this setup, overall network connectivity is controlled by adjusting the presence of red–red links, π_{rr} . Fig. 3(a–d) shows the size of the giant component for networks with

the same Coleman index $h = 0.3$, but different values of h_2 and h_6 , which reflect varying levels of across- and within-group homophily.

When red–blue links are partially kept, $\pi_{rb} > 0$, panels (a) and (b), red and blue nodes can form a joint giant component altogether. Even with the same Coleman index h , networks with higher across-group homophily h_2 yield larger giant components at high π_{rr} . Therefore, local mixing patterns affect not only the size of the giant component but also when the percolation transition happens, revealing structural effects that measures like the Coleman index miss. When red–blue links are absent, $\pi_{rb} = 0$, percolation can occur only through nodes of the same color, thus the size of the giant component is limited by the number of red or blue nodes. Different combinations of h_2 and h_6 modify the percolation threshold. In panel (d), where $\pi_{bb} = 0.2$, the giant component begins growing at the same threshold as in panel (c) ($\pi_{bb} = 0$), but from a higher baseline—indicating that percolation already occurs through blue–blue links, regardless of red–red links. Panel (a) shows that a large cluster emerges regardless of red–red links whenever a fraction of red–blue and blue–blue links are active. In panel (b), percolation thresholds are lower than in panel (c), due to the presence of across-group links. These results show that local mixing patterns affect not only the size of the giant component but also when the percolation transition happens, revealing structural effects that measures like the Coleman index miss.

B. Critical percolation value

Analytical solutions for percolation on non-tree-like networks are famously intractable [107, 108]; yet, by isolating within-clique spreading from across-clique behavior, our framework breaks this impasse and provides a closed-form expression for the critical percolation threshold (see Section V F). Using a multi-type branching process, we show that the percolation vector $\boldsymbol{\pi} = (\pi_{rr}, \pi_{rb}, \pi_{bb})$ is critical when there exists a non-negative vector \boldsymbol{v} such that

$$\boldsymbol{v} \in \ker(\mathbf{B}(\boldsymbol{\pi}) - \mathbf{I}), \quad \boldsymbol{v}/|\boldsymbol{v}| \geq 0, \quad (9)$$

where \mathbf{I} is the identity matrix and the matrix $\mathbf{B} = \mathbf{B}(\boldsymbol{\pi})$ (see Eq. (20) in Methods) encodes the expected number of nodes of a given clique type reached from another via percolation. The condition $\det(\mathbf{B}(\boldsymbol{\pi}) - \mathbf{I}) = 0$ is necessary but not sufficient for criticality. In expression (9), $\ker(\cdot)$ denotes the kernel (null space) of a matrix—i.e., the set of vectors mapped to zero—and $\det(\cdot)$ is the determinant, indicating when the matrix becomes singular.

We explore this condition in networks parametrized by within-group homophily h_4 and across-group homophily h_2 . Fig. 4(a–b) shows heatmaps of the critical value $\pi_{rr} = \pi_{bb}$ for different values of π_{rb} . When π_{rb} is low (Fig. 4a), increasing the global homophily expressed by the Coleman index h reduces the critical threshold. When π_{rb} is high (Fig. 4b), increasing h instead raises the threshold. Interestingly, these figures reveal how group homophilies

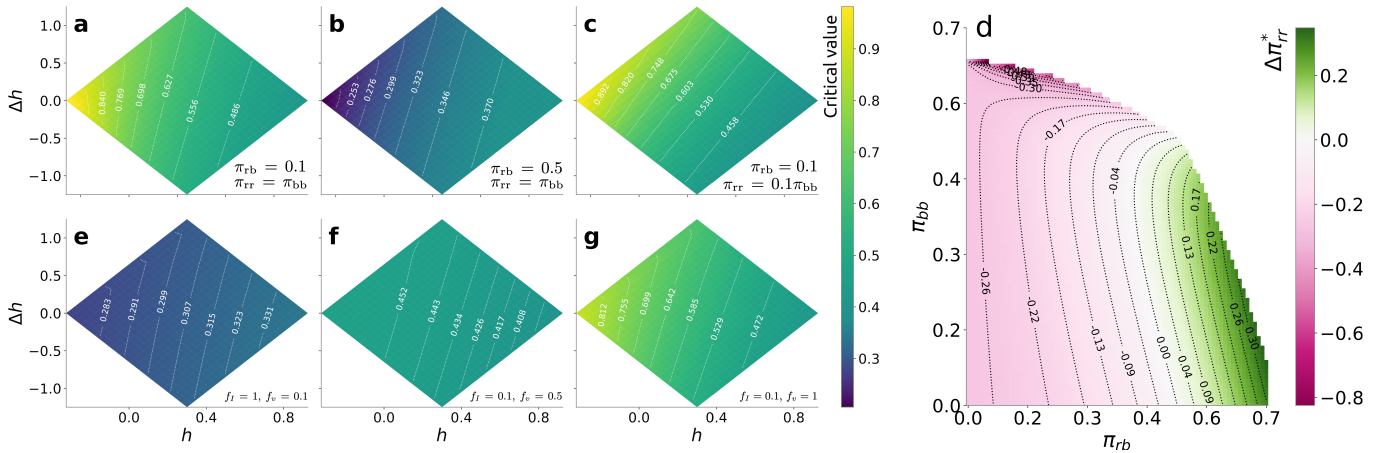


FIG. 4. **Within- and across-group Homophily Influences Network Connectivity, Percolation Properties and Epidemic Thresholds in Non-Uniform Ways.** Panels (a–c) present heatmaps of the critical percolation value with respect to $h = (h_2 + h_4)/2$ and $\Delta h = h_2 - h_4$ for: (a) $\pi_{rr} = \pi_{bb}$, $\pi_{rb} = 0.1$; (b) $\pi_{rr} = \pi_{bb}$, $\pi_{rb} = 0.5$; (c) $\pi_{rr} = 0.1\pi_{bb}$, $\pi_{rb} = 0.1$, $\alpha = 0.2$. These panels illustrate how redistributing homophily configurations can either raise or lower the percolation threshold depending on the extent of across-group connectivity π_{rb} . Panel (d) compares the effect of redistributing homophily across small and large groups in networks with $h = 0.5$ and average degree 2. Green regions indicate that emphasizing small-group homophily ($h_4 = 0.1$, $h_2 = 0.9$) leads to a higher percolation threshold than emphasizing large-group homophily ($h_2 = 0.1$, $h_4 = 0.9$). No percolation transition occurs in the top-right white region. Panels (e–g) explore the interaction between homophily and vaccination efficacy with respect to $h = (h_2 + h_4)/2$ and $\Delta h = h_2 - h_4$. The impact of homophily depends on both within-group efficacy (f_v) and cross-group efficacy (f_I): (e) $f_I = 1$, $f_v = 0.1$; (f) $f_I = 0.1$, $f_v = 0.5$; (g) $f_I = 0.1$, $f_v = 1$.

affect connectivity, even when the Coleman index is fixed. We see that level curves for the critical value $\pi_{rr} = \pi_{bb}$ are not vertically aligned, meaning that for fixed h , distinct combinations of h_2 and h_4 yield different percolation thresholds. In particular, when π_{rb} is low, percolation is more easily achieved if $h_4 > h_2$; vice versa, when π_{rb} is high, the percolation threshold is lower if $h_2 > h_4$. The importance of local homophily is more prominent when $\pi_{rr} \neq \pi_{bb}$, as depicted in Fig. 4c. Here, the contour lines are roughly diagonal, indicating that the type of homophily is equally important to the amount of homophily for the percolation threshold. This means that the type of homophily can have a significant impact on the critical value of π_{rr} , which can range from 0.4 to 0.75 even when the Coleman homophily h remains fixed.

To illustrate the role of homophily within and across groups for the percolation threshold more systematically, we fix $h = 0.5$ with $\alpha = 0.5$ and compare two configurations: (i) weak across-group homophily ($h_2 = 0.1$) and strong within-group homophily ($h_4 = 0.9$), and (ii) the reverse. We compute the difference in critical values: $\Delta\pi_{rr}^* = \pi_{rr}^*(h_4 = 0.1) - \pi_{rr}^*(h_2 = 0.1)$. Fig. 4d shows that this difference can be either positive or negative, depending on π_{rb} and π_{bb} . Increasing the connectivity between groups (higher π_{rb}) enhances the effectiveness of across-group homophily in maintaining network connectivity. In other words, when many cross-group links are present, networks with stronger across-group homophily achieve percolation at lower thresholds compared to networks with stronger within-group homophily. Thus, stronger homophily within or across groups does not universally

improve connectivity. The difference in critical π_{rr} values between networks with the same Coleman index can be as large as 0.8, showing that global homophily alone is insufficient to predict percolation behavior.

C. Epidemic Spread & Vaccination

We demonstrate how multiscale homophily influences epidemic dynamics by applying our percolation framework to contact networks. Homophily affects disease transmission through vaccination behaviors and demographic mixing patterns alike. Age serves as a prime example: empirical contact matrices consistently show strong age-assortative mixing, with children primarily interacting with other children and adults exhibiting distinct interaction patterns depending on age and context [100–104]. Such structured contacts significantly reshape infection pathways, thereby affecting key epidemiological outcomes including herd immunity thresholds, expected epidemic sizes, and the effectiveness of interventions [14, 25, 26]. Our framework facilitates a detailed analysis of intervention strategies, providing a foundation for improved design and interpretation of public health policies [109]. To illustrate this, we analyze a vaccination scenario involving an imperfect vaccine, categorizing individuals as vaccinated (red) and unvaccinated (blue) nodes, to investigate how homophily shapes disease spread and influences the success of interventions.

With perfect vaccines, only red–red links remain active, and any link involving at least one vaccinated node

is removed from the transmission network. However, with imperfect vaccines, vaccinated individuals can still transmit the disease, though at a reduced value, to both vaccinated and unvaccinated individuals compared to the baseline probability π between two unvaccinated nodes. If the across-group vaccine efficacy f_I reduces transmission between vaccinated and unvaccinated individuals, and the within-group efficacy f_v reduces transmission across vaccinated individuals, then the transmission probabilities are $\pi_{rb} = f_I\pi$ and $\pi_{bb} = f_v\pi$, respectively [14].

Fig. 4(e-g) shows that the impact of f_I and f_v on the critical percolation threshold is non-trivial. As in Fig. 4(a-c), the effect of homophily on the critical value can reverse. In Fig. 4e, increasing either homophily raises the critical threshold, while in Fig. 4g, it lowers it. This mirrors earlier results: for low π_{rb} , increasing homophily decreases the critical value. Since $\pi_{rb} = f_I\pi$, the values of f_I in these panels explain the observed shift— $\pi_{rb} = \pi$ in Fig. 4e and 0.1π in Fig. 4g. Fig. 4f shows that for certain combinations of f_I and f_v , the critical value becomes nearly insensitive to either form of homophily.

In tree-like networks, the required vaccine coverage for herd immunity increases with the Coleman index h , and high homophily may render herd immunity unattainable [14]. Our results reveal that layered homophily creates far more complex outcomes. For example, in Fig. 4g, the critical threshold ranges from 0.5 to 0.64 when the Coleman homophily remains fixed at $h = 0.5$, a 30% difference, highlighting the influence of homophily structure on epidemic dynamics and intervention outcomes.

V. CONCLUSION & DISCUSSION

We have introduced a flexible framework for capturing homophily across multiple social scales, combining tightly knit subgroups with across-group interactions. By applying a maximum-entropy approach to maximal clique decomposition, our model accurately replicates homophily patterns in diverse real-world datasets, demonstrating how these trends remain hidden when homophily is considered as a single parameter. We further show that homophily may raise or lower percolation thresholds depending on the interaction between within- and across-group percolation, demonstrating that carefully tuned interventions (e.g., targeted vaccination or social distancing) can yield different outcomes. The connectivity insights provided by our framework remain applicable to any spreading phenomenon that can be effectively represented as a percolation process. Thus, our multiscale homophily decomposition provides a principled foundation for analyzing phenomena ranging from information diffusion to countering misinformation by managing link activation within and across groups.

We note that while our model specifically addresses homophilic interactions, it omits other key structural features of social networks, such as degree heterogeneity or degree correlations. This simplification helps isolate the

specific effects of group homophily, making the model particularly useful as a null model. Networks that share similar group sizes and homophily levels, yet exhibit additional characteristics like degree heterogeneity, can be compared against our model to determine whether observed differences arise from structural features beyond homophily. Thus, our framework serves to clarify whether empirical patterns are solely driven by homophily or if other structural elements also play a significant role.

Nevertheless, the model can readily incorporate additional constraints on node degrees or hyperedge structures due to its underlying exponential-family formulation, allowing easy customization to empirical data. Furthermore, this flexibility extends naturally to scenarios where homophily parameters evolve over time presents a streamlined yet flexible approach for analyzing multiscale homophily, laying the groundwork for future studies that incorporate multiple attributes per node, capturing interactions between attributes that may result in non-additive effects, such as decreased homophily in one dimension influencing homophily in another [110]. Overall, this work presents a streamlined yet flexible approach for analyzing multiscale homophily, laying the groundwork for future studies that incorporate richer dynamics, degree heterogeneity, and higher-order motifs. This versatility enhances our understanding of how local assortative interactions influence global connectivity across social, biological, and technological networks, prompting further experimental and computational exploration into the broader implications of homophily-like biases in complex systems.

Although our focus has been on social networks, our method can be applied to other systems with “like-likes-like” biases. Polymer or colloidal assemblies, for example, involve monomer or particle species whose binding preferences mirror within-group homophily [111–113], and neural networks often exhibit connectivity shaped by neuron type or layer [114, 115]. Likewise, in gene regulatory or protein–protein interaction networks, functionally similar nodes tend to cluster [116–119]. In each of these contexts, our maximum-entropy model could provide a systematic way to assess how local mixing biases influence an entire system.

Our decomposition of homophily reveals that what appears as modest or even absent assortativity at the network level often conceals a spectrum of structured, group-size-dependent mixing patterns. This observation challenges prevailing modeling assumptions and calls for a more elaborate understanding of how homophily operates in social systems and the implications for the various dynamics on them. By capturing this previously hidden structure in homophily patterns, our framework not only offers better alignment with empirical observations but also provides a principled model for investigating the behavior of dynamical processes on social networks.

ACKNOWLEDGMENTS

Funding: AKR acknowledges support from the Independent Research Fund Denmark (EliteForsk grant to Sune Lehmann), the Carlsberg Foundation (The Hope Project), and the Villum Foundation (NationScale Social networks). CS is supported by an NWO VENI grant 202.001. MK acknowledges the grant number 349366 from the Research Council of Finland. The simulations presented above were performed using computer resources within the Aalto University School of Science’s “Science-IT” project.

Use of AI tools: We utilized AI language tools to enhance grammar and readability. The authors reviewed and approved all content.

Competing interests: The authors declare no competing interests.

Data and materials availability: All essential simulations and numerical computations are publicly available at [120]. The datasets used in this project were gathered from other research papers. Data collection methods, network details, and attribute distributions are provided in the original papers.

-
- [1] M. McPherson, L. Smith-Lovin, and J. M. Cook, Birds of a feather: Homophily in social networks, *Annual review of sociology* **27**, 415 (2001).
- [2] M. E. Newman, Assortative mixing in networks, *Physical review letters* **89**, 208701 (2002).
- [3] M. E. Newman, The structure and function of complex networks, *SIAM review* **45**, 167 (2003).
- [4] R. Noldus and P. Van Mieghem, Assortativity in complex networks, *Journal of Complex Networks* **3**, 507 (2015).
- [5] G. T. Cantwell and M. Newman, Mixing patterns and individual differences in networks, *Physical Review E* **99**, 042306 (2019).
- [6] J. Moody, Race, school integration, and friendship segregation in america, *American journal of Sociology* **107**, 679 (2001).
- [7] C. Beyrer, S. D. Baral, F. Van Griensven, S. M. Goodreau, S. Chariyalertsak, A. L. Wirtz, and R. Brookmeyer, Global epidemiology of hiv infection in men who have sex with men, *The Lancet* **380**, 367 (2012).
- [8] S. A. Staras, R. L. Cook, and D. B. Clark, Sexual partner characteristics and sexually transmitted diseases among adolescents and young adults, *Sexually transmitted diseases* **36**, 232 (2009).
- [9] G. Kossinets and D. J. Watts, Origins of homophily in an evolving social network, *American journal of sociology* **115**, 405 (2009).
- [10] A. Endo, H. Murayama, S. Abbott, R. Ratnayake, C. A. Pearson, W. J. Edmunds, E. Fearon, and S. Funk, Heavy-tailed sexual contact networks and monkeypox epidemiology in the global outbreak, 2022, *Science* **378**, 90 (2022).
- [11] E. P. Griggs, B. Flannery, I. M. Foppa, M. Gaglani, K. Murthy, M. L. Jackson, L. A. Jackson, E. A. Belongia, H. Q. McLean, E. T. Martin, *et al.*, Role of age in the spread of influenza, 2011–2019: data from the us influenza vaccine effectiveness network, *American Journal of Epidemiology* **191**, 465 (2022).
- [12] C. J. Worby, S. S. Chaves, J. Wallinga, M. Lipsitch, L. Finelli, and E. Goldstein, On the relative role of different age groups in influenza epidemics, *Epidemics* **13**, 10 (2015).
- [13] C. J. Worby, C. Kenyon, R. Lynfield, M. Lipsitch, and E. Goldstein, Examining the role of different age groups and of vaccination during the 2012 minnesota pertussis outbreak, *Scientific reports* **5**, 13182 (2015).
- [14] T. Hiraoka, A. K. Rizi, M. Kivelä, and J. Saramäki, Herd immunity and epidemic size in networks with vaccination homophily, *Physical Review E* **105**, L052301 (2022).
- [15] C. J. E. Metcalf, K. Hampson, A. J. Tatem, B. T. Grenfell, and O. N. Bjørnstad, Persistence in epidemic metapopulations: quantifying the rescue effects for measles, mumps, rubella and whooping cough, *PloS one* **8**, e74696 (2013).
- [16] S. Aral, L. Muchnik, and A. Sundararajan, Distinguishing influence-based contagion from homophily-driven diffusion in dynamic networks, *Proceedings of the National Academy of Sciences* **106**, 21544 (2009).
- [17] M. Kalmijn, Inter-marriage and homogamy: Causes, patterns, trends, *Annual review of sociology* **24**, 395 (1998).
- [18] V. A. Lewis, Social energy and racial segregation in the university context, *Social Science Quarterly* **93**, 270 (2012).
- [19] E. Bakshy, S. Messing, and L. A. Adamic, Exposure to ideologically diverse news and opinion on facebook, *Science* **348**, 1130 (2015).
- [20] J. Tacchi, C. Boldrini, A. Passarella, and M. Conti, Keep your friends close, and your enemies closer: Structural properties of negative relationships on twitter, *arXiv:2401.16562* (2024).
- [21] H. Pei, B. Wei, K. C.-C. Chang, Y. Lei, and B. Yang, Geom-gcn: Geometric graph convolutional networks, *arXiv:2002.05287* (2020).
- [22] J. Zhu, Y. Yan, L. Zhao, M. Heimann, L. Akoglu, and D. Koutra, Beyond homophily in graph neural networks: Current limitations and effective designs, *Advances in neural information processing systems* **33**, 7793 (2020).
- [23] Y. Ma, X. Liu, N. Shah, and J. Tang, Is homophily a necessity for graph neural networks?, *arXiv:2106.06134* (2021).
- [24] Y. Zheng, S. Luan, and L. Chen, What is missing in homophily? disentangling graph homophily for graph neural networks, *arXiv:2406.18854* (2024).
- [25] A. K. Rizi, A. Faqeeh, A. Badie-Modiri, and M. Kivelä, Epidemic spreading and digital contact tracing: Effects of heterogeneous mixing and quarantine failures, *Physical Review E* **105**, 044313 (2022).
- [26] A. K. Rizi, L. A. Keating, J. P. Gleeson, D. J. O’Sullivan, and M. Kivelä, Effectiveness of contact tracing on networks with cliques, *Physical Review E* **109**, 024303 (2024).
- [27] T. Hiraoka, A. K. Rizi, Z. Ghadiri, M. Kivelä, and J. Saramäki, The strength and weakness of disease-induced herd immunity, *arXiv:2307.04700* (2023).
- [28] L. Hébert-Dufresne, S. V. Scarpino, and J.-G. Young, Macroscopic patterns of interacting contagions are indis-

- tinguishable from social reinforcement, *Nature Physics* **16**, 426 (2020).
- [29] L. Hébert-Dufresne, T. M. Waring, G. St-Onge, M. T. Niles, L. Kati Corlew, M. P. Dube, S. J. Miller, N. J. Gotelli, and B. J. McGill, Source-sink behavioural dynamics limit institutional evolution in a group-structured society, *Royal Society Open Science* **9**, 211743 (2022).
- [30] L. H. Nguyen, D. A. Drew, M. S. Graham, A. D. Joshi, C.-G. Guo, W. Ma, R. S. Mehta, E. T. Warner, D. R. Sikavi, C.-H. Lo, *et al.*, Risk of covid-19 among front-line health-care workers and the general community: a prospective cohort study, *The Lancet Public Health* **5**, e475 (2020).
- [31] G. Shirreff, B.-T. Huynh, A. Duval, L. C. Pereira, D. Annane, A. Dinh, O. Lambotte, S. Bulifon, M. Guichardon, S. Beaune, *et al.*, Assessing respiratory epidemic potential in french hospitals through collection of close contact data (april–june 2020), *Scientific Reports* **14**, 3702 (2024).
- [32] L. Temime, M.-P. Gustin, A. Duval, N. Buetti, P. Crepey, D. Guillemot, R. Thiébaud, P. Vanhems, J.-R. Zahar, D. R. Smith, *et al.*, A conceptual discussion about the basic reproduction number of severe acute respiratory syndrome coronavirus 2 in healthcare settings, *Clinical Infectious Diseases* **72**, 141 (2021).
- [33] J. Wallinga, P. Teunis, and M. Kretzschmar, Using data on social contacts to estimate age-specific transmission parameters for respiratory-spread infectious agents, *American journal of epidemiology* **164**, 936 (2006).
- [34] R. M. Anderson and R. M. May, *Infectious diseases of humans: dynamics and control* (Oxford university press, 1991).
- [35] C. Geismar, P. J. White, A. Cori, and T. Jombart, Sorting out assortativity: When can we assess the contributions of different population groups to epidemic transmission?, *Plos one* **19**, e0313037 (2024).
- [36] A. K. Rizzi, *Spreading and Epidemic Interventions - Effects of Network Structure and Dynamics*, Ph.d. thesis, Aalto University (2024).
- [37] S. Cure, F. G. Pflug, and S. Pigolotti, Exponential rate of epidemic spreading on complex networks, *Physical Review E* **111**, 044311 (2025).
- [38] M. S. Granovetter, The strength of weak ties, *American journal of sociology* **78**, 1360 (1973).
- [39] M. Granovetter, The strength of weak ties: A network theory revisited, *Sociological theory*, 201 (1983).
- [40] J. Mou, L. Wang, K. Wen, B. Dai, S. Tan, F. Liljeros, P. Holme, and X. Lu, Quantifying the weakness of ties with hierarchy-based link centrality, *Science China Information Sciences* **68**, 192202 (2025).
- [41] A. Rapoport, Contribution to the theory of random and biased nets, *The bulletin of mathematical biophysics* **19**, 257 (1957).
- [42] A. Porter and I. Rafols, Is science becoming more interdisciplinary? measuring and mapping six research fields over time, *Scientometrics* **81**, 719 (2009).
- [43] M. Á. Serrano, M. Boguñá, and A. Vespignani, Patterns of dominant flows in the world trade web, *Journal of Economic Interaction and Coordination* **2**, 111 (2007).
- [44] Y.-A. Pignolet, S. Schmid, and A. Seelisch, Gender-specific homophily on instagram and implications on information spread, *Scientific Reports* **14**, 451 (2024).
- [45] L. Gallo, C. Zappalà, F. Karimi, and F. Battiston, Higher-order modeling of face-to-face interactions, arXiv:2406.05026 (2024).
- [46] D. Laniado, Y. Volkovich, K. Kappler, and A. Kaltenbrunner, Gender homophily in online dyadic and triadic relationships, *EPJ Data Science* **5**, 19 (2016).
- [47] S. Sajjadi, S. Martin-Gutierrez, and F. Karimi, Unveiling homophily beyond the pool of opportunities, arXiv preprint arXiv:2401.13642 (2024).
- [48] L. Peel, J.-C. Delvenne, and R. Lambiotte, Multiscale mixing patterns in networks, *Proceedings of the National Academy of Sciences* **115**, 4057 (2018).
- [49] M. Granovetter, The impact of social structure on economic outcomes, *Journal of Economic Perspectives*, 19 (1), 33-50 (2005).
- [50] M. Bojanowski and R. Corten, Measuring segregation in social networks, *Social networks* **39**, 14 (2014).
- [51] F. Battiston, E. Amico, A. Barrat, G. Bianconi, G. Ferraz de Arruda, B. Franceschiello, I. Iacopini, S. Kéfi, V. Latora, Y. Moreno, *et al.*, The physics of higher-order interactions in complex systems, *Nature Physics* **17**, 1093 (2021).
- [52] N. Apollonio, P. G. Franciosa, and D. Santoni, A novel method for assessing and measuring homophily in networks through second-order statistics, *Scientific reports* **12**, 9757 (2022).
- [53] N. Veldt, A. R. Benson, and J. Kleinberg, Combinatorial characterizations and impossibilities for higher-order homophily, *Science Advances* **9**, eabq3200 (2023).
- [54] F. Karimi and M. Oliveira, On the inadequacy of nominal assortativity for assessing homophily in networks, *Scientific Reports* **13**, 21053 (2023).
- [55] N. C. Grassly and C. Fraser, Mathematical models of infectious disease transmission, *Nature Reviews Microbiology* **6**, 477 (2008).
- [56] S. M. Goodreau, J. A. Kitts, and M. Morris, Birds of a feather, or friend of a friend? using exponential random graph models to investigate adolescent social networks, *Demography* **46**, 103 (2009).
- [57] L. Hébert-Dufresne, A. Allard, J.-G. Young, and L. J. Dubé, Percolation on random networks with arbitrary k-core structure, *Physical Review E* **88**, 062820 (2013).
- [58] R. S. Burt, Structural holes, in *Social stratification* (Routledge, 2018) pp. 659–663.
- [59] L. Hébert-Dufresne, B. M. Althouse, S. V. Scarpino, and A. Allard, Beyond $r=0$: heterogeneity in secondary infections and probabilistic epidemic forecasting, *Journal of the Royal Society Interface* **17**, 20200393 (2020).
- [60] P. W. Holland, K. B. Laskey, and S. Leinhardt, Stochastic blockmodels: First steps, *Social networks* **5**, 109 (1983).
- [61] M. M. Egbert, Schisming: The collaborative transformation from a single conversation to multiple conversations, *Research on Language and Social Interaction* **30**, 1 (1997).
- [62] I. Iacopini, M. Karsai, and A. Barrat, The temporal dynamics of group interactions in higher-order social networks, *Nature Communications* **15**, 7391 (2024).
- [63] J. S. Coleman, *Relational Analysis: The Study of Social Organizations with Survey Methods*, *Human Organization* **17**, 28 (1958).
- [64] J. S. Coleman, *Introduction to Mathematical Sociology* (Free Press of Glencoe, New York, 1964) pp. xiv, 554.
- [65] M. E. Newman, Mixing patterns in networks, *Physical*

- review E **67**, 026126 (2003).
- [66] M. E. Newman and M. Girvan, Finding and evaluating community structure in networks, *Physical review E* **69**, 026113 (2004).
- [67] H. Narimanzadeh, T. Hiraoka, and M. Kivelä, Block-corrected modularity for community detection, arXiv:2502.20083 (2025).
- [68] A. Salloum, T. H. Y. Chen, and M. Kivelä, Separating polarization from noise: comparison and normalization of structural polarization measures, *Proceedings of the ACM on human-computer interaction* **6**, 1 (2022).
- [69] M. Piraveenan, M. Prokopenko, and A. Zomaya, Local assortativeness in scale-free networks, *Europhysics Letters* **84**, 28002 (2008).
- [70] M. Piraveenan, M. Prokopenko, and A. Y. Zomaya, On congruity of nodes and assortative information content in complex networks, *Networks and Heterogeneous Media* **7**, 441 (2012).
- [71] D. Sivia and J. Skilling, *Data analysis: a Bayesian tutorial* (OUP Oxford, 2006).
- [72] M. Kardar, *Statistical physics of fields* (Cambridge University Press, 2007).
- [73] F.-Y. Wu, The potts model, *Reviews of modern physics* **54**, 235 (1982).
- [74] J. Cardy, *Scaling and renormalization in statistical physics*, Vol. 5 (Cambridge university press, 1996).
- [75] L. Takac and M. Zabovsky, Data analysis in public social networks, in *International scientific conference and international workshop present day trends of innovations*, Vol. 1 (2012).
- [76] P. Sapiezynski, A. Stopczynski, D. D. Lassen, and S. Lehmann, Interaction data from the copenhagen networks study, *Scientific Data* **6**, 315 (2019).
- [77] A. Asikainen, G. Iñiguez, J. Ureña-Carrión, K. Kaski, and M. Kivelä, Cumulative effects of triadic closure and homophily in social networks, *Science Advances* **6**, eaax7310 (2020).
- [78] J.-P. Onnela, J. Saramäki, J. Hyvönen, G. Szabó, D. Lazer, K. Kaski, J. Kertész, and A.-L. Barabási, Structure and tie strengths in mobile communication networks, *Proceedings of the National Academy of Sciences* **104**, 7332 (2007), <https://www.pnas.org/doi/pdf/10.1073/pnas.0610245104>.
- [79] A. Asikainen, G. Iñiguez, K. Kaski, and M. Kivelä, Cumulative effects of triadic closure and homophily in social networks, arXiv:1809.06057 (2018).
- [80] C. Cattuto, W. Van den Broeck, A. Barrat, V. Colizza, J.-F. Pinton, and A. Vespignani, Dynamics of person-to-person interactions from distributed rfid sensor networks, *PLoS one* **5**, e11596 (2010).
- [81] A. L. Traud, P. J. Mucha, and M. A. Porter, Social structure of facebook networks, *Physica A: Statistical Mechanics and its Applications* **391**, 4165 (2012).
- [82] K. M. Altenburger and J. Ugander, Monophily in social networks introduces similarity among friends-of-friends, *Nature human behaviour* **2**, 284 (2018).
- [83] I. Smirnov, S. Thurner, M. Schläpfer, and A. Garas, Academic performance drives the restructuring of friendship networks in school, *PLoS ONE* **12**, e0183473 (2017).
- [84] Z. Boda and B. Néray, Inter-ethnic friendship and negative ties in secondary school, *Social Networks* **43**, 57 (2015).
- [85] M. Newman, *Networks* (Oxford university press, 2018).
- [86] N. Araújo, P. Grassberger, B. Kahng, K. Schrenk, and R. M. Ziff, Recent advances and open challenges in percolation, *The European Physical Journal Special Topics* **223**, 2307 (2014).
- [87] A. Hackett, D. Cellai, S. Gómez, A. Arenas, and J. P. Gleeson, Bond percolation on multiplex networks, *Physical Review X* **6**, 021002 (2016).
- [88] G. Bianconi, Epidemic spreading and bond percolation on multilayer networks, *Journal of Statistical Mechanics: Theory and Experiment* **2017**, 034001 (2017).
- [89] H. Sun, F. Radicchi, J. Kurths, and G. Bianconi, The dynamic nature of percolation on networks with triadic interactions, *Nature Communications* **14**, 1308 (2023).
- [90] J.-P. Onnela, J. Saramäki, J. Hyvönen, G. Szabó, D. Lazer, K. Kaski, J. Kertész, and A.-L. Barabási, Structure and tie strengths in mobile communication networks, *Proceedings of the national academy of sciences* **104**, 7332 (2007).
- [91] H. Schawe, S. Fontaine, and L. Hernández, When network bridges foster consensus. bounded confidence models in networked societies, *Physical Review Research* **3**, 023208 (2021).
- [92] C. Moore and M. E. Newman, Epidemics and percolation in small-world networks, *Physical Review E* **61**, 5678 (2000).
- [93] R. Pastor-Satorras and A. Vespignani, Epidemic spreading in scale-free networks, *Physical review letters* **86**, 3200 (2001).
- [94] M. E. Newman, Spread of epidemic disease on networks, *Physical review E* **66**, 016128 (2002).
- [95] S. N. Dorogovtsev, A. V. Goltsev, and J. F. Mendes, Critical phenomena in complex networks, *Reviews of Modern Physics* **80**, 1275 (2008).
- [96] L. H.-D. et. al., One pathogen does not an epidemic make: A review of interacting contagions, diseases, beliefs, and stories (2025), arXiv:2504.15053v1.
- [97] E. Goldstein, M. Lipsitch, and M. Cevik, On the effect of age on the transmission of sars-cov-2 in households, schools, and the community, *The Journal of infectious diseases* **223**, 362 (2021).
- [98] C. Tran Kiem, P. Bosetti, J. Paireau, P. Crepey, H. Salje, N. Lefrancq, A. Fontanet, D. Benamouzig, P.-Y. Boëlle, J.-C. Desenclos, et al., Sars-cov-2 transmission across age groups in france and implications for control, *Nature communications* **12**, 6895 (2021).
- [99] J. Roy, S. M. Heath, S. Wang, and D. Ramkrishna, Modeling covid-19 transmission between age groups in the united states considering virus mutations, vaccinations, and reinfection, *Scientific Reports* **12**, 20098 (2022).
- [100] J. Mossong, N. Hens, M. Jit, P. Beutels, K. Auranen, R. Mikolajczyk, M. Massari, S. Salmaso, G. S. Tomba, J. Wallinga, et al., Social contacts and mixing patterns relevant to the spread of infectious diseases, *PLoS medicine* **5**, e74 (2008).
- [101] I. Osei, E. Mendy, K. van Zandvoort, B. Young, O. Jobe, G. Sarwar, N. I. Mohammed, J. Bruce, B. Greenwood, S. Flasche, et al., Social contacts and mixing patterns in rural gambia, *BMC infectious diseases* **25**, 243 (2025).
- [102] K. Prem, A. R. Cook, and M. Jit, Projecting social contact matrices in 152 countries using contact surveys and demographic data, *PLoS computational biology* **13**, e1005697 (2017).
- [103] N. G. Davies, P. Klepac, Y. Liu, K. Prem, M. Jit, and R. M. Eggo, Age-dependent effects in the transmission and control of covid-19 epidemics, *Nature medicine* **26**,

- 1205 (2020).
- [104] J. Zhang, M. Litvinova, Y. Liang, Y. Wang, W. Wang, S. Zhao, Q. Wu, S. Merler, C. Viboud, A. Vespignani, *et al.*, Changes in contact patterns shape the dynamics of the covid-19 outbreak in china, *Science* **368**, 1481 (2020).
- [105] I. Kryven, Bond percolation in coloured and multiplex networks, *Nature communications* **10**, 404 (2019).
- [106] L. Cirigliano and C. Castellano, Neighbor-induced damage percolation, *Physical Review E* **111**, 054312 (2025).
- [107] M. Mezard and A. Montanari, *Information, physics, and computation* (Oxford University Press, 2009).
- [108] M. Newman, Message passing methods on complex networks, *Proceedings of the Royal Society A* **479**, 20220774 (2023).
- [109] J. St-Onge, G. Burgio, S. F. Rosenblatt, T. M. Waring, and L. Hébert-Dufresne, Paradoxes in the coevolution of contagions and institutions, *Proceedings of the Royal Society B* **291**, 20241117 (2024).
- [110] P. Block and T. Grund, Multidimensional homophily in friendship networks, *Network Science* **2**, 189 (2014).
- [111] L. A. Navarro, J. J. Ryan, M. Dzuricky, M. Gradzielski, A. Chilkoti, and S. Zauscher, Microphase separation of resilin-like and elastin-like diblock copolypeptides in concentrated solutions, *Biomacromolecules* **22**, 3827 (2021).
- [112] J. J. Karnes, T. H. Weisgraber, J. S. Oakdale, M. Mettry, M. Shusteff, and J. Biener, On the network topology of cross-linked acrylate photopolymers: a molecular dynamics case study, *The Journal of Physical Chemistry B* **124**, 9204 (2020).
- [113] Z. Zeravcic, V. N. Manoharan, and M. P. Brenner, Size limits of self-assembled colloidal structures made using specific interactions, *Proceedings of the National Academy of Sciences* **111**, 15918 (2014).
- [114] A. Azulay, E. Itskovits, and A. Zaslaver, The *c. elegans* connectome consists of homogenous circuits with defined functional roles, *PLoS computational biology* **12**, e1005021 (2016).
- [115] A. B. Kunin, J. Guo, K. E. Bassler, X. Pitkow, and K. Josić, Hierarchical modular structure of the drosophila connectome, *Journal of Neuroscience* **43**, 6384 (2023).
- [116] W. Yin, L. Mendoza, J. Monzon-Sandoval, A. O. Urrutia, and H. Gutierrez, Emergence of co-expression in gene regulatory networks, *PloS one* **16**, e0247671 (2021).
- [117] A. K. Rizi, M. Zamani, A. Shirazi, G. R. Jafari, and J. Kertész, Stability of imbalanced triangles in gene regulatory networks of cancerous and normal cells, *Frontiers in Physiology* **11**, 573732 (2021).
- [118] S. Navlakha and C. Kingsford, The power of protein interaction networks for associating genes with diseases, *Bioinformatics* **26**, 1057 (2010).
- [119] N. Apollonio, P. G. Franciosa, and D. Santoni, On function homophily of microbial protein-protein interaction networks., *CoRR* (2021).
- [120] Github repository, <https://github.com/k-rizi/Homophily-Within-Across-Groups>.

METHODS

A. Fitting the Model to Data

Given an empirical network, we identify all maximal cliques, group them by size c , and derive an empirical distribution representing the proportion of cliques containing different numbers of red nodes. We then assume a maximum entropy distribution for clique configurations—constrained by the observed number of red nodes per clique and the overall homophily index—and infer the parameters θ_r and θ_{h_c} of Eq. (8) by maximizing the likelihood of the observed distributions.

To ensure robust estimates, we employ a bootstrap resampling procedure for each clique size, drawing the same number of cliques 1,000 times and computing mean homophily values and 95% confidence intervals. Error bars in Fig. 2b are the bootstrap confidence intervals.

B. Link Duplication

In large, sparse networks where cliques rarely overlap, Eq. (3) (the Coleman index) and Eq. (6) (the clique-based homophily formula) are equivalent. However, in finite-size empirical networks, c -cliques often share links, leading to redundancy. In a network G_c , the number of links, denoted by L_c , is always less than or equal to the total number of links in the M_c maximal c -cliques. The duplication ratio captures the extent of this redundancy

$$\delta_c = 1 - \frac{2L_c}{M_c c(c-1)}, \quad (10)$$

where higher δ_c indicates greater link-sharing among cliques. When δ_c is small, we can approximate the actual fraction of same-color links by expanding around the nominal (no-overlap) value:

$$e_{kk} = e_{kk}^{(c)} + \gamma_{kk} \delta_c + \mathcal{O}(\delta_c^2), \quad (11)$$

where $k \in \{b, r\}$ and the coefficients γ_{kk} capture how color-biased the overlap is: if duplication disproportionately affects red-red links, then $\gamma_{kk} \neq 0$, etc. The difference in the same color duplicated links will be

$$(e_{rr} + e_{bb}) - (e_{rr}^{(c)} + e_{bb}^{(c)}) = \gamma \delta_c + \mathcal{O}(\delta_c^2), \quad (12)$$

with $\gamma = \gamma_{rr} + \gamma_{bb}$.

Substituting into Eq. (3) yields

$$H = h_c + \frac{\gamma \delta_c}{1 - n_r^2 - n_b^2} + \mathcal{O}(\delta_c^2). \quad (13)$$

Hence, if duplication is *color-unbiased* ($\gamma = 0$), the overlap does not alter homophily at first order, implying

$$H = h_c + \mathcal{O}(\delta_c^2) \approx h_c. \quad (14)$$

c	M_c	δ_c	h_c	h'_c
2	208,463	0.00	$-0.02^{+0.01}_{-0.01}$	0.00
3	67,930	0.20	$0.20^{+0.01}_{-0.01}$	0.19
4	25,651	0.31	$0.25^{+0.01}_{-0.01}$	0.22
5	10,472	0.39	$0.26^{+0.01}_{-0.01}$	0.22
6	4,293	0.49	$0.27^{+0.02}_{-0.02}$	0.22
7	1,888	0.55	$0.28^{+0.02}_{-0.02}$	0.23
8	824	0.61	$0.35^{+0.03}_{-0.03}$	0.30
9	357	0.71	$0.36^{+0.05}_{-0.05}$	0.29
10	116	0.66	$0.29^{+0.09}_{-0.08}$	0.33

TABLE II. **Effect of Link Duplications on Homophily in the Last.fm Network.** The duplication ratio δ_c is computed for the empirical data and is expected to be zero for a network generated using Last.fm statistics. The homophily values h_c and H_c are computed for G_c using (6) and (3), respectively. Error values represent bootstrap confidence intervals. The similarity between these values supports the approximation in (14).

Conversely, a nonzero γ indicates color-biased overlap, shifting the actual Coleman index away from the nominal h_c by roughly $\gamma\delta_c$.

When measuring the duplication ratio in an empirical network, a larger variance in node degrees can lead to a higher duplication ratio as the likelihood of the same link appearing in multiple maximal cliques increases. High-degree nodes participate in many cliques, and if their neighbors also belong to overlapping groups, shared links are counted repeatedly. In contrast, in networks where node degrees are more uniform, the chances of a link being reused across multiple cliques are lower. Additionally, if the network exhibits positive degree assortativity, where high-degree nodes preferentially connect to other high-degree nodes, this effect is further amplified, leading to even greater duplication.

Table II shows that in practice Eq. (14) holds. Eq. (3) is best suited for measuring homophily directly from the adjacency matrix, making it useful for assessing network-wide segregation, while Eq. (6) provides a more refined approach for parameter inference in clique-based models, such as the maximum-entropy distribution of clique compositions.

C. Aggregating Node Statuses

Consider a discrete spectrum of colors where we aim to combine s colors into $S < s$ colors. We can achieve this by merging certain original colors using the mapping function

$$\varphi : \{1, \dots, s\} \rightarrow \{1, \dots, S\},$$

which assigns each original color k a new “merged” color $\varphi(k)$. Say, all shades of blue to blue. After this identification, the *new* distribution $\tilde{F}_{(j_1, \dots, j_S)}$ must sum all the

old probabilities $F_{(i_1, \dots, i_s)}$ whose indices (i_1, \dots, i_s) agree with the merged color counts $\mathbf{j} = (j_1, \dots, j_S)$.

$$\tilde{F}_{(j_1, \dots, j_S)} = \sum_{\substack{i_1 + \dots + i_s = c \\ j_\alpha = \sum_{k: \varphi(k) = \alpha} i_k}} F_{(i_1, \dots, i_s)},$$

This procedure *lumps* together all old configurations whose new color composition is \mathbf{j} . Although \tilde{F} is a valid probability distribution, it typically does *not* remain in the same exponential-family form unless every group of merged colors was already indistinguishable in the exponent. In other words, the original parameters (like θ_k) and any homophily function must treat those merged colors *identically* for the sum to factor neatly. In that *renormalizable* scenario, the new \tilde{F} preserves the same functional shape. This coarse-graining remains an exponential family without further re-fitting if the original model assigned *identical* roles to those merged categories. Otherwise, one must solve a new maximum-entropy problem in the reduced color space, and any notion of homophily now reflects only these broader, less granular labels. This is analogous to lumping the s -state Potts model into $S = 2$ (red vs. blue), which does not necessarily result in a simple Ising model with the standard coupling [73, 74].

D. Beyond Two Colors

In the definition of h_c in Eq (6) and in Section II B, we have focused on networks where nodes possess binary attributes, such as male and female or red and blue, for the sake of simplicity. However, this framework can be extended to nodes with discrete states or categorical attributes. Each clique network G_c , and consequently the mixed clique network $G = \bigcup G_c$, can be extended to a multi-color version. Different colors may represent different social groups, features, or functionalities within the network. Assume that each node has one of $s \geq 1$ different colors, then $\binom{c+s-1}{s-1}$ different c -clique types and hence $s(s+1)/2$ different link types can be present.

The number of nodes of each color is denoted by N_k where $k = 1, \dots, s$, while their fraction over the total number of nodes N is denoted by n_k . For fixed clique size c , each clique type can be uniquely specified by a vector $\mathbf{i} = (i_1, \dots, i_s)$ encoding the number of nodes of each color in the clique. For example, if $s = 3$ (red, blue, or green nodes) and $c = 4$, the vector $(2, 1, 1)$ corresponds to the 4-clique with 2 red nodes, 1 blue node, and 1 green node. Similarly, as in the 2-color case, different cliques yield different homophily indices,

$$h_{\mathbf{i}} = \frac{\binom{i_1 + \dots + i_s}{c} - (n_1^2 + \dots + n_s^2)}{1 - (n_1^2 + \dots + n_s^2)}. \quad (15)$$

M_c cliques are sampled according to a given distribution vector F_c , where $F_{c,i}$ specifies the probability of selecting a particular clique type. Again, we constrain G_c to achieve

a desired network homophily value h , and assume that all different color nodes have the same expected degree, similarly to Eq. (1). This yields the maximum entropy clique distribution

$$F_i = \frac{1}{Z} \exp \left(\sum_{k=1}^{s-1} \theta_k i_k + \lambda h_i \right). \quad (16)$$

The exponents $\theta_1, \dots, \theta_{s-1}$ are conjugated to the constraints that ensure the average proportion of colored nodes in the cliques matches the total proportion of colored cliques. Instead, λ is specified after requiring the desired homophily network value h . The constraints read explicitly as

$$N_k = \frac{1}{c} \sum_{\mathbf{i}} i_k F_{\mathbf{i}}, \quad k = 1, \dots, s-1 \quad (17)$$

$$h = \sum_{\mathbf{i}} h_i F_{\mathbf{i}}. \quad (18)$$

Similarly, as in the 2-colored version, a multi-layer structured network can be obtained when mixing cliques of different sizes.

E. Multidimensional Homophily: Beyond Colors

Consider nodes characterized by multiple discrete attributes (e.g., color and temperature). To describe cliques, we define a composition vector \mathbf{I} , where each element \mathbf{I}_j indicates the number of nodes in the clique with attribute combination j , satisfying $\sum_{j=1}^c \mathbf{I}_j = c$. Under the maximum-entropy framework, the probability distribution generalizes naturally to:

$$F_{c,\mathbf{I}} = \frac{1}{Z} \exp \left(\sum_k \theta_k \phi_k(\mathbf{I}) \right),$$

where the statistics $\{\phi_k\}$ encode relevant constraints (such as homophily per attribute or interactions between attributes), and the conjugate parameters $\{\theta_k\}$ enforce these constraints.

F. Critical percolation value

To analyze the critical percolation value analytically, we map the percolation process on the clique network to a percolation process on a tree-like network by analyzing the spreading within the clique separately from the behavior across cliques. We therefore calculate the average number of infected I' -cliques caused by a percolated node in an I -clique.

The average number of type I -cliques that are adjacent to a randomly chosen red or blue node equals

$$F_{r,I}^* := M_{c(I)} \frac{n_{r,I} F_I}{N_r}, \quad F_{b,I}^* := M_{c(I)} \frac{n_{b,I} F_I}{N_b}, \quad (19)$$

where $n_{r,I}, n_{b,I}$ denote the number of red, blue nodes in a type I clique, and $M_{c(I)}$ the total number of cliques of the same size as I . Furthermore, let $\boldsymbol{\pi} = [\pi_{rr}, \pi_{rb}, \pi_{bb}]$ be the values quantifying the probabilities that red-red, red-blue, and blue-blue links are kept active after percolation. Finally, let $g_r(I, \boldsymbol{\pi}, n_r, n_b)$ denote the probability that, after percolation, a randomly chosen red node is still connected to n_r red and n_b blue nodes within the same clique of type I ; similarly, $g_b(I, \boldsymbol{\pi}, n_r, n_b)$ denotes the probability that a randomly chosen blue node remains connected to n_r and n_b nodes within I .

Then, the average number of type I' cliques that are reached after percolation from a node of color $(*) \in \{r, b\}$ from a red node in a clique of type I equals

$$B_{I_r, I'_{(*)}} = F_{(*), I'}^* \sum_{n_b=0}^{n_{b,I}} \sum_{n_r=1}^{n_{r,I}} (n_{(*)} - \delta_{r,(*)}) g_r(I, \boldsymbol{\pi}, n_r, n_b). \quad (20)$$

The term inside the inner summation is the average number of nodes of color $(*)$ in the I -clique that are still connected to the red node after percolation. The term in front is the average number of type I' cliques adjacent to $(*)$ colored nodes. The average number of I' cliques reached at a color $(*)$ node from a blue node in I is denoted by $B_{I_b, I'_{(*)}}$, and it is calculated similarly.

Therefore, the matrix $\mathbf{B} = \mathbf{B}(\boldsymbol{\pi})$ encodes the average number of nodes of specific clique types that are reached through percolation starting within another specific clique type. Then a percolation vector $\boldsymbol{\pi}$ is critical when there is a vector \mathbf{v} , for which

$$\mathbf{v} \in \ker[\mathbf{B}(\boldsymbol{\pi}) - \mathbf{I}], \quad \mathbf{v}/|\mathbf{v}| \geq 0, \quad (21)$$

where \mathbf{I} denotes the identity matrix. Note that $\det(\mathbf{B}(\boldsymbol{\pi}) - \mathbf{I}) = 0$ is a necessary condition for this to hold.

The elements of the matrix \mathbf{B} require the probabilities $g_b(I, \boldsymbol{\pi}, n_r, n_b)$ and $g_r(I, \boldsymbol{\pi}, n_r, n_b)$. For any clique of type I with $n_{r,I}$ red nodes and $n_{b,I}$ blue nodes, the probability that the clique remains connected after percolation is $g_b(I, \boldsymbol{\pi}, n_{r,I}, n_{b,I}) = g_r(I, \boldsymbol{\pi}, n_{r,I}, n_{b,I})$. This probability equals one minus the probability that there exists a cut in the clique, and can be written recursively as

$$\begin{aligned} g_b(I, \boldsymbol{\pi}, n_{r,I}, n_{b,I}) &= 1 - \sum_{j=1}^{n_{b,I}} \sum_{i=0}^{n_{r,I}} \binom{n_{b,I}-1}{j-1} \binom{n_{r,I}}{i} \\ &\times g_b(I_{i,j}, \boldsymbol{\pi}, i, j) (1 - \pi_{rr})^{i(d_r-i)} \\ &\times (1 - \pi_{bb})^{j(d_b-j)} (1 - \pi_{br})^{i(d_b-j)+j(d_r-i)}, \quad (22) \end{aligned}$$

$$\begin{aligned} g_r(I, \boldsymbol{\pi}, n_{r,I}, n_{b,I}) &= 1 - \sum_{j=0}^{n_{b,I}} \sum_{i=1}^{n_{r,I}} \binom{n_{b,I}}{j} \binom{n_{r,I}-1}{i-1} \\ &\times g_b(I_{i,j}, \boldsymbol{\pi}, i, j) (1 - \pi_{rr})^{i(d_r-i)} \\ &\times (1 - \pi_{bb})^{j(d_b-j)} (1 - \pi_{br})^{i(d_b-j)+j(d_r-i)}. \quad (23) \end{aligned}$$

From these equations, we can compute $g_b(I, \boldsymbol{\pi}, n_r, n_b)$ when $n_r \leq n_{r,I}$ or $n_b \leq n_{b,I}$, as

$$\begin{aligned} g_b(I, \boldsymbol{\pi}, n_r, n_b) &= \binom{n_{b,I} - 1}{n_b - 1} \binom{n_{r,I}}{n_r} g_b(I_{n_r, n_b}, \boldsymbol{\pi}, n_r, n_b) \\ &\times (1 - \pi_{rr})^{n_r(n_{r,I} - n_r)} (1 - \pi_{bb})^{n_b(n_{b,I} - n_b)} \\ &\times (1 - \pi_{br})^{n_r(n_{b,I} - n_b) + n_b(n_{r,I} - n_r)}, \end{aligned} \quad (24)$$

$$\begin{aligned} g_r(I, \boldsymbol{\pi}, n_r, n_b) &= \binom{n_{b,I}}{n_b} \binom{n_{r,I} - 1}{n_r - 1} g_r(I_{n_r, n_b}, \boldsymbol{\pi}, n_r, n_b) \\ &\times (1 - \pi_{rr})^{n_r(n_{r,I} - n_r)} (1 - \pi_{bb})^{n_b(n_{b,I} - n_b)} \\ &\times (1 - \pi_{br})^{n_r(n_{b,I} - n_b) + n_b(n_{r,I} - n_r)}. \end{aligned} \quad (25)$$

These equations take the probability that a clique with n_r and n_b red and blue nodes remains connected from Eq. (22) and (23), and multiplies it with the probability that these nodes are not connected to any remaining nodes of the clique.